Title
The structure of a contact-dependent growth-inhibition (CDI) immunity protein from Neisseria meningitidis MC58

Journal
Acta Crystallographica Section F: Structural Biology Communications, 71(6)

ISSN
2053-230X

Authors
Tan, Kemin
Johnson, Parker M
Stols, Lucy
et al.

Publication Date
2015-06-01

DOI
10.1107/s2053230x15006585

Peer reviewed

STRUCTURAL BIOLOGY COMMUNICATIONS

ISSN 2053-230X

The structure of a contact-dependent growth-inhibition (CDI) immunity protein from *Neisseria meningitidis* MC58

Kemin Tan,[a,b] Parker M. Johnson,[c] Lucy Stols,[a] Bryan Boubion,[c] William Eschenfeldt,[a] Gyorgy Babnigg,[a] Christopher S. Hayes,[d,e] Andrezj Joachimiak[a,b] and Celia W. Goulding[c,f]*

[a]Midwest Center for Structural Genomics, Argonne National Laboratory, Argonne, IL 60439, USA, [b]Structural Biology Center, Biosciences, Argonne National Laboratory, Argonne, IL 60439, USA, [c]Department of Molecular Biology and Biochemistry, University of California Irvine, Irvine, CA 92697, USA, [d]Department of Molecular, Cellular and Developmental Biology, University of California Santa Barbara, Santa Barbara, CA 93106, USA, [e]Biomolecular Science and Engineering Program, University of California Santa Barbara, Santa Barbara, CA 93106, USA, and [f]Department of Pharmaceutical Sciences, University of California Irvine, Irvine, CA 92697, USA. *Correspondence e-mail: celia.goulding@uci.edu

Received 9 February 2015
Accepted 31 March 2015

Edited by T. C. Terwilliger, Los Alamos National Laboratory, USA

Keywords: contact-dependent growth inhibition; CdiA-CT toxin domain; CdiI immunity protein; toxin–immunity protein complex; *Neisseria meningitidis*; docking studies.

PDB reference: CdiI immunity protein, 4q7o

Supporting information: this article has supporting information at journals.iucr.org/f

Contact-dependent growth inhibition (CDI) is an important mechanism of intercellular competition between neighboring Gram-negative bacteria. CDI systems encode large surface-exposed CdiA effector proteins that carry a variety of C-terminal toxin domains (CdiA-CTs). All CDI$^+$ bacteria also produce CdiI immunity proteins that specifically bind to the cognate CdiA-CT and neutralize its toxin activity to prevent auto-inhibition. Here, the X-ray crystal structure of a CdiI immunity protein from *Neisseria meningitidis* MC58 is presented at 1.45 Å resolution. The CdiI protein has structural homology to the Whirly family of RNA-binding proteins, but appears to lack the characteristic nucleic acid-binding motif of this family. Sequence homology suggests that the cognate CdiA-CT is related to the eukaryotic EndoU family of RNA-processing enzymes. A homology model is presented of the CdiA-CT based on the structure of the XendoU nuclease from *Xenopus laevis*. Molecular-docking simulations predict that the CdiA-CT toxin active site is occluded upon binding to the CdiI immunity protein. Together, these observations suggest that the immunity protein neutralizes toxin activity by preventing access to RNA substrates.

1. Introduction

Bacteria have developed several complex mechanisms to interact and communicate with neighboring microbes in the environment. One such mechanism is contact-dependent growth inhibition (CDI), a form of interbacterial competition found in several important human pathogens including uropathogenic *Escherichia coli*, *Burkholderia pseudomallei* and *Neisseria meningitidis* (Aoki *et al.*, 2011). CDI is mediated by the CdiB/CdiA family of two-partner secretion proteins. CdiB is an outer membrane β-barrel protein that exports and displays the CdiA effector protein on the surface of CDI$^+$ inhibitor cells (Aoki *et al.*, 2005). CdiA proteins are very large, ranging from 180 kDa to over 600 kDa depending on the bacterial species, and are characterized by hemagglutinin-peptide repeats that suggest a filamentous structure (Kajava *et al.*, 2001). CdiA proteins are predicted to extend several hundred angstroms from the surface of inhibitor cells to interact with specific receptors on the surface of susceptible target bacteria. Upon contact with its receptor, CdiA delivers a toxin domain derived from its extreme C-terminus (CdiA-CT) into the target bacterium (Aoki *et al.*, 2010; Ruhe *et al.*,

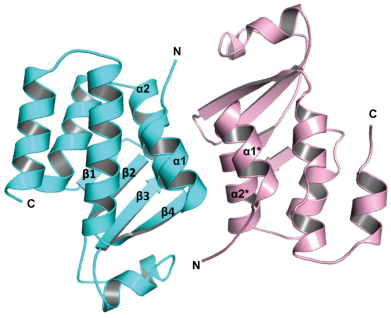

2014). CdiA-CT toxins vary considerably between bacteria and even between different strains of the same species (Aoki *et al.*, 2010). This sequence diversity corresponds to a variety of toxin activities ranging from the formation of membrane pores to the degradation of ribosomal RNA (Ruhe *et al.*, 2013). CDI^+ bacteria protect themselves from auto-inhibition by expressing CdiI immunity proteins, which bind to the CdiA-CT domain and neutralize its toxin activity. CdiI immunity proteins are specific for their cognate CdiA-CT and do not protect cells from the toxins of other CDI^+ bacteria. Thus, CDI systems encode a complex network of toxin–immunity protein pairs that are deployed for intercellular competition.

N. meningitidis is a parasitic, aerobic, Gram-negative bacterium responsible for pyogenic meningitis and meningococcal septicemia. It is a major cause of disease worldwide, resulting in hearing loss, brain damage and death in 4–10% of sufferers (Thigpen *et al.*, 2011; Nikulin *et al.*, 2006). Every year, approximately 3000–4000 cases of *N. meningitidis*-linked meningitis are reported in the United States (Thigpen *et al.*, 2011). Because this pathogen poses a serious threat to global health, a greater understanding of its growth control could be leveraged to develop novel therapeutics targeted specifically to *Neisseria*. All *N. meningitidis* isolates carry at least one CDI system, and some strains have multiple complex loci that contain two *cdiA* genes and tandem arrays of 'orphan' *cdiA-CT*/*cdiI* gene pairs (Bentley *et al.*, 2007; Poole *et al.*, 2011). Orphan *cdiA-CT* gene fragments often share significant regions of homology with the upstream *cdiA* gene and therefore can undergo homologous recombination to fuse the orphan *cdiA-CT*/*cdiI* module onto *cdiA*. This process can abruptly change the toxin deployed by the cell (Koskiniemi *et al.*, 2014). The large number of CDI-associated toxin/immunity genes carried by *N. meningitidis* suggests that these systems mediate interstrain competition. This hypothesis is supported by a recent study by Tommassen and coworkers (Arenas *et al.*, 2013). Here, we report the crystal structure of $CdiI_{o2}^{MC58\text{-}1}$, an orphan CDI immunity protein from *N. meningitidis* MC58. In addition, we have generated structural models for the cognate CdiA-$CT_{o2}^{MC58\text{-}1}$ toxin and its corresponding toxin–immunity protein complex.

2. Materials and methods

2.1. Cloning of the *N. meningitidis* CdiA-$CT_{o2}^{MC58\text{-}1}$/$CdiI_{o2}^{MC58\text{-}1}$ genes

A fragment containing NMB0502 and NBM0503 (encoding CdiA-$CT_{o2}^{MC58\text{-}1}$ and $CdiI_{o2}^{MC58\text{-}1}$, respectively) was amplified from *N. meningitidis* MC58 genomic DNA using 5′ -GTC TCT CCC ATG GTG AAA AAT AAT CAG CTT AGC GAC AAA GAG as the forward primer and 5′ -TGG TGG TGC CCA GCG GTT TCA TGC AGG CTA CAG TTT GTT TGA as the reverse primer. The gel-purified PCR product was treated with phage T4 DNA polymerase and dTTP as described previously (Eschenfeldt *et al.*, 2010) and ligated to plasmid pMCSG58, which appends a noncleavable His_6 tag to the C-terminus of $CdiI_{o2}^{MC58\text{-}1}$ (Eschenfeldt *et al.*, 2013). The identity of the cloned insert was confirmed by DNA sequencing.

2.2. Expression and purification of *N. meningitidis* $CdiI_{o2}^{MC58\text{-}1}$

The construct was introduced into *E. coli* BL21 (DE3) cells for overexpression and protein purification. The cells were grown at 37°C in LB medium supplemented with 100 µg ml^{-1} ampicillin. After the cells had grown to an optical density at 600 nm of ∼0.6, the culture was cooled to 18°C and protein expression was induced with 0.5 m*M* isopropyl *β*-D-1-thiogalactopyranoside (IPTG) overnight. Under these growth conditions, only the $CdiI_{o2}^{MC58\text{-}1}$ immunity protein was overproduced. The cells were harvested by centrifugation, resuspended in 50 m*M* Tris pH 8.0, 500 m*M* NaCl, 10 m*M* *β*-mercaptoethanol (BME), 10% glycerol and lysed with Fast Break reagent (Promega) containing 10 µg ml^{-1} lysozyme and protease-inhibitor cocktail (Roche). The cell lysate was centrifuged at 10 000 rev min^{-1} for 1 h and the supernatant was passed through a 0.22 µm filter. The clarified lysate was then loaded onto an Ni^{2+}-Sepharose HisTrap column (GE Healthcare) and proteins were eluted with a 20–250 m*M* linear gradient of imidazole in resuspension buffer. Fractions were pooled and loaded onto a HiLoad 26/60 Superdex 75 size-exclusion column equilibrated with 20 m*M* Tris pH 7.5, 150 m*M* NaCl, 2 m*M* dithiothreitol. Fractions containing purified $CdiI_{o2}^{MC58\text{-}1}$ immunity protein were pooled and concentrated for crystallization using an Amicon Ultra centrifugal filter device with a 3000 Da cutoff (Millipore).

2.3. Size-exclusion chromatography

Analysis of the purified $CdiI_{o2}^{MC58\text{-}1}$ was performed using a Dionex HPLC system with an analytical size-exclusion column from Sepax (SRT-SEC-150, Sepax Technologies). $CdiI_{o2}^{MC58\text{-}1}$ was diluted to 5 mg ml^{-1} in standard running buffer (20 m*M* Tris pH 7.8, 150 m*M* NaCl, 2 m*M* dithiothreitol). The sample-injection volume was 20 µl and the flow rate of the analysis was 1.0 ml min^{-1}. $CdiI_{o2}^{MC58\text{-}1}$ was run in duplicate. Each run took approximately 15 min. The molecular-weight determination of $CdiI_{o2}^{MC58\text{-}1}$ was calculated using linear regression data analysis with ovalbumin (44 kDa), carbonic anhydrase (29 kDa) and ribonuclease A (13.7 kDa) as migration standards.

2.4. Crystallization of the $CdiI_{o2}^{MC58\text{-}1}$ immunity protein

Native $CdiI_{o2}^{MC58\text{-}1}$ crystals were grown at 4°C using sitting drops that consisted of 10 mg ml^{-1} protein in 0.2 *M* $MgCl_2$, 0.1 *M* bis-tris pH 5.5, 20% PEG 3350. Bromide derivatives were prepared by dipping crystals into a solution of 1.0 *M* KBr, 0.2 *M* $MgCl_2$, 0.1 *M* bis-tris pH 5.5, 20% PEG 3350, 15% glycerol for approximately 10 s. Bromide-derivatized crystals were subsequently cryocooled in liquid nitrogen and used to collect X-ray diffraction data for phase determination (Dauter *et al.*, 2000).

2.5. X-ray data collection, structure determination and refinement

A set of single-wavelength anomalous diffraction (SAD) data was collected near the bromine absorption peak (12.40 keV) at 100 K from one $CdiI_{o2}^{MC58\text{-}1}$ crystal. Data were obtained on the 19-ID beamline of the Structural Biology Center at the Advanced Photon Source at Argonne National Laboratory using the *SBCcollect* program (Rosenbaum *et al.*, 2006). Data-set intensities were integrated, scaled and merged using the *HKL*-3000 program suite (Minor *et al.*, 2006; Table 1). From the Matthews correlation coefficient, two $CdiI_{o2}^{MC58\text{-}1}$ molecules were predicted in one asymmetric unit. 17 Br sites were located using *SHELXD* (Sheldrick, 2008) and were used for phasing with *MLPHARE* from *CCP*4 (Winn *et al.*, 2011). After density modification, a partial model of 138 residues (46% of a dimer) without side chains was built in three cycles of *ARP*/*wARP* model building (Cohen *et al.*, 2004). All of the abovementioned programs are integrated within the *HKL*-3000 suite (Minor *et al.*, 2006). The final $CdiI_{o2}^{MC58\text{-}1}$ model was completed manually using *Coot* (Emsley & Cowtan, 2004) and was refined with *phenix.refine* (Afonine *et al.*, 2012) (Table 1).

2.6. Expression and purification of the *N. meningitidis* $CdiA\text{-}CT_{o2}^{MC58\text{-}1}$–$CdiI_{o2}^{MC58\text{-}1}$ complex

The construct from §2.1 was introduced into *E. coli* BL21 (DE3) cells and grown at 37°C in LB medium supplemented with 100 µg ml^{-1} ampicillin. After the cells had grown to an optical density at 600 nm of ∼0.8, protein expression was induced with 1.5 m*M* IPTG for 2.5 h at 37°C. The cells were harvested by centrifugation and resuspended in 20 m*M* Tris pH 8.0, 150 m*M* NaCl, 10 m*M* BME, 1 m*M* phenylmethylsulfonyl fluoride, 10 µg ml^{-1} lysozyme. The cells were lysed using a microfluidizer and centrifuged at 10 000 rev min^{-1} for 1 h and the supernatant was passed through a 0.22 µm filter. The clarified lysate was then loaded onto Ni^{2+}–NTA resin (GE Healthcare) and nonspecifically bound proteins were eluted with resuspension buffer with no BME and 20 m*M* imidazole under gravity. The imidazole concentration was increased to 250 m*M* to elute the toxin–immunity protein complex.

2.7. Docking of predicted toxin and immunity proteins

A model of the $CdiA\text{-}CT_{o2}^{MC58\text{-}1}$–$CdiI_{o2}^{MC58\text{-}1}$ binding interaction was generated through docking simulations. A computational model of the $CdiA\text{-}CT_{o2}^{MC58\text{-}1}$ structure was generated with *Sculptor* (Birmanns *et al.*, 2011) using the three-dimensional structure of the homologous XendoU nuclease (PDB entry 2c1w; Renzi *et al.*, 2006) as a guide. The $CdiA\text{-}CT_{o2}^{MC58\text{-}1}$ sequence was fitted into the XendoU structure while maintaining the overall fold and alignment of the predicted active-site histidine residues.

Hex 8.0 (Macindoe *et al.*, 2010) was used to dock the $CdiI_{o2}^{MC58\text{-}1}$ immunity protein onto the *Sculptor*-modeled $CdiA\text{-}CT_{o2}^{MC58\text{-}1}$ structure. The proteins were oriented and the origins were set to allow free rotation of the two molecules during the search for low-energy binding interactions based on complementary shape and electrostatics. Energies for each model were calculated by adding all intermolecular interactions after a round of molecular-mechanics energy minimization. Typical Hex simulations produce binding energies of −600 to −1000 kcal mol^{-1} (Gupta *et al.*, 2013). A control docking simulation using $CdiA\text{-}CT^{EC536}$ toxin and CysK, which are known to interact (Diner *et al.*, 2012), generated a low energy of interaction of −988 kcal mol^{-1}. Simulations for proteins that do not interact (*E. coli* CysK and *B. pseudomallei* E479 CdiI; Nikolakakis *et al.*, 2012) yielded a much higher energy of −368 kcal mol^{-1}.

Table 1
Data-collection and crystallographic statistics for $CdiI_{o2}^{MC58\text{-}1}$.

Values in parentheses are for the last resolution bin.

Data collection	
Space group	$P2_1$
Unit-cell parameters (Å, °)	a = 45.38, b = 53.53, c = 59.70, β = 98.04
Molecular weight† (Da)	16727
No. of residues†	143
Molecules in asymmetric unit	2
Wavelength (Å)	0.9193 [Br peak]
Resolution (Å)	30.0–1.45 (1.48–1.45)
No. of unique reflections	49973‡
Multiplicity	3.4 (2.2)
Completeness (%)	99.5 (94.9)
R_{merge} (%)	10.7 (38.4)
$\langle I/\sigma(I)\rangle$	24.4 (2.3)
Solvent content (%)	41.7
Phasing	
R_{Cullis} (anomalous) (%)	89
Figure of merit (%)	19.4§
Refinement	
Resolution (Å)	30.0–1.45
No. of reflections (work/test)	47390/2544
R_{cryst}/R_{free} (%)	14.9/18.9
R.m.s. deviations from ideal geometry	
Bond lengths (Å)	0.005
Bond angles (°)	0.967
No. of atoms	
Protein	2229
Heteroatoms	300
Mean B value (Å^2)	
Main chain	11.25
Side chain	14.24
Ramachandran plot statistics, residues in (%)	
Most favored regions	93.0
Additional allowed region	7.0
Generously allowed regions	0
Disallowed region	0
PDB code	4q7o

† Not including a three-residue N-terminal tag, SNA. ‡ Including Bijvoet pairs. § Before density modification.

3. Results and discussion

3.1. Overall structure of $CdiI_{o2}^{MC58\text{-}1}$

$CdiI_{o2}^{MC58\text{-}1}$ crystallized in space group $P2_1$ with two molecules in the asymmetric unit. The structure was determined using a bromide derivative and SAD phasing, and the final model was refined to a resolution of 1.45 Å (Table 1).

The $CdiI_{o2}^{MC58\text{-}1}$ structure represents an α/β-fold comprising a four-stranded antiparallel β-sheet, against which a five-helix bundle is packed (Fig. 1*a*). The helical bundle includes three

helices (α1–α3) from the N-terminus and two (α5 and α6) from the C-terminus. Additionally, there are two consecutive helices with one short 3_{10}-helix (colored blue in Fig. 1*a*) followed by another short α-helix (α4) within a large loop that connects strands β2 and β3. Helix α4 is located on the edge of the β-sheet on the face opposite to the helical bundle and close to the C-terminus. With the exception of the surface interacting with the large loop, the remainder of one face of the β-sheet is completely exposed to solvent.

Within the asymmetric unit, CdiI$_{o2}^{MC58\text{-}1}$ appears to form a nearly perfect noncrystallographic twofold-symmetric dimer, with helices α1 and α2 from each monomer packed against

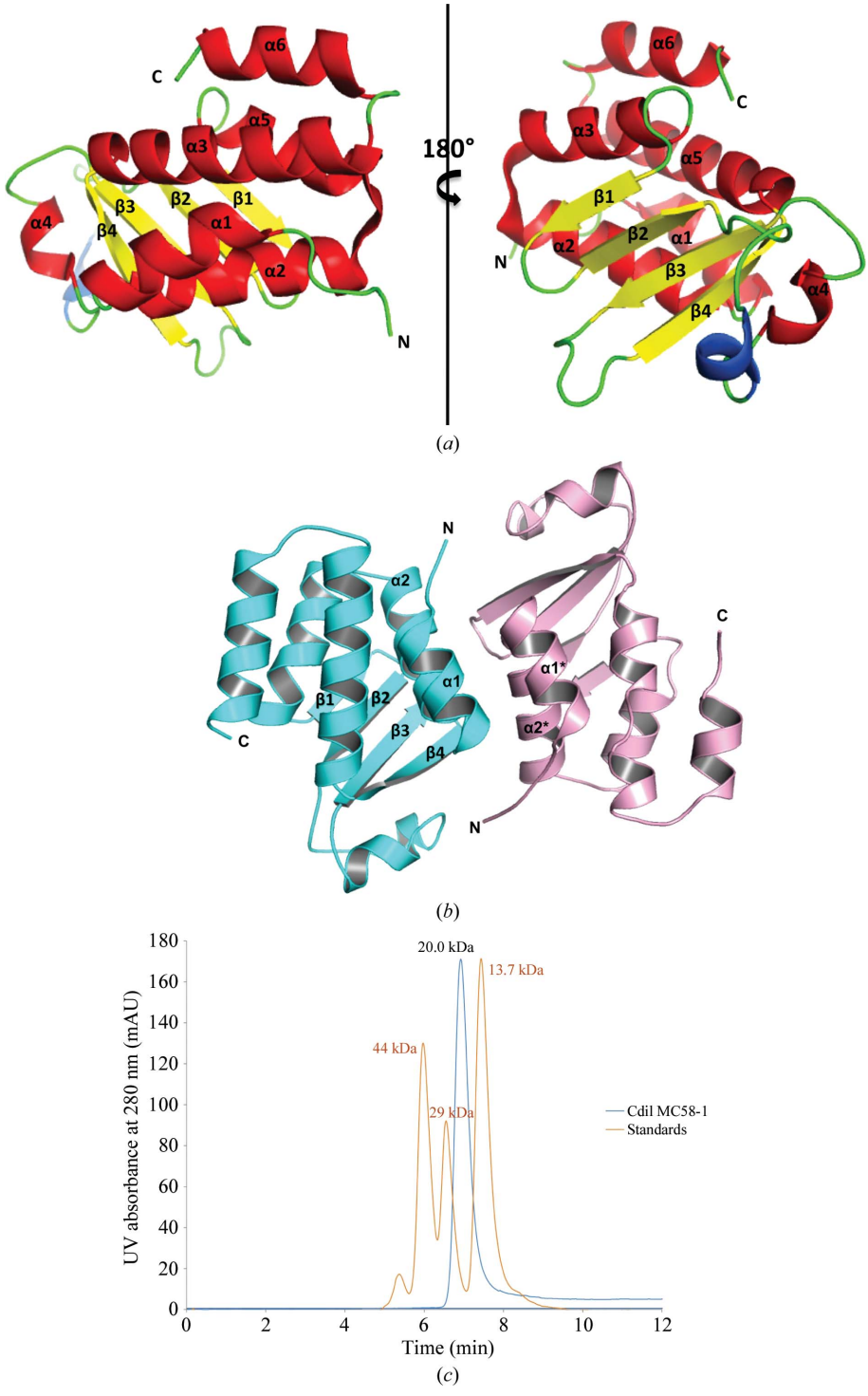

Figure 1
(*a*) Ribbon cartoon of the CdiI$_{o2}^{MC58\text{-}1}$ structure with α-helices, β-strands and the 3_{10}-helix colored red, yellow and blue, respectively. (*b*) The interface produced by helices α1 and α2 from each monomer in the asymmetric unit. (*c*) Analytical size-exclusion chromatography using an SRT-SEC-150 column suggests that CdiI$_{o2}^{MC58\text{-}1}$ (blue trace; standards, orange trace) is monomeric in solution.

each other in an antiparallel mode (Fig. 1*b*). This type of helical bundle is a common structural motif at protein–protein interfaces (Norel *et al.*, 1995). The buried surface area owing to dimerization is about 1065 Å^2 per monomer as determined by *PDBePISA* (Krissinel & Henrick, 2007). To test whether CdiI$_{o2}^{MC58\text{-}1}$ is dimeric in solution, we analyzed the immunity protein by analytical size-exclusion chromatography and found it to be predominately monomeric (Fig. 1*c*). Thus, the dimeric assembly observed in the crystal structure is perhaps an artifact of crystallization.

3.2. Structural comparison

CdiI$_{o2}^{MC58\text{-}1}$ has moderate structural similarity to two eukaryotic nucleic acid-binding proteins. The closest structural homolog, as determined using the *DALI* server (Holm *et al.*, 2008), is a mitochondrial Whirly protein (Why2; PDB entry 4kop) from *Arabidopsis thaliana* (Cappadocia *et al.*, 2013), and CdiI$_{o2}^{MC58\text{-}1}$ superimposes upon Why2 with an r.m.s.d. of 2.5 Å over 80 of 145 C$^{\alpha}$ atoms (Figs. 2*a*, 2*b* and 2*d*). Whirly family members are single-stranded DNA-binding proteins that modulate DNA repair in plant chloroplasts (Cappadocia *et al.*, 2010; Desveaux *et al.*, 2005). The next closest structural homolog is mitochondrial RNA-binding protein 1 (MRP1; PDB entry 2gia) from *Trypanosoma brucei* (Schumacher *et al.*, 2006), and MRP1 superimposes onto CdiI$_{o2}^{MC58\text{-}1}$ with an r.m.s.d. of 3.0 Å over 85 of 132 C$^{\alpha}$ atoms (Figs. 2*c* and 2*e*). MRP1 forms a heterotetramer with MRP2, and together the two proteins function in RNA editing by promoting the hybridization to guide RNAs to their target mRNAs (Aphasizhev *et al.*, 2003). Although the top structural homologs are nucleic acid-binding proteins, CdiI$_{o2}^{MC58\text{-}1}$ lacks the structural

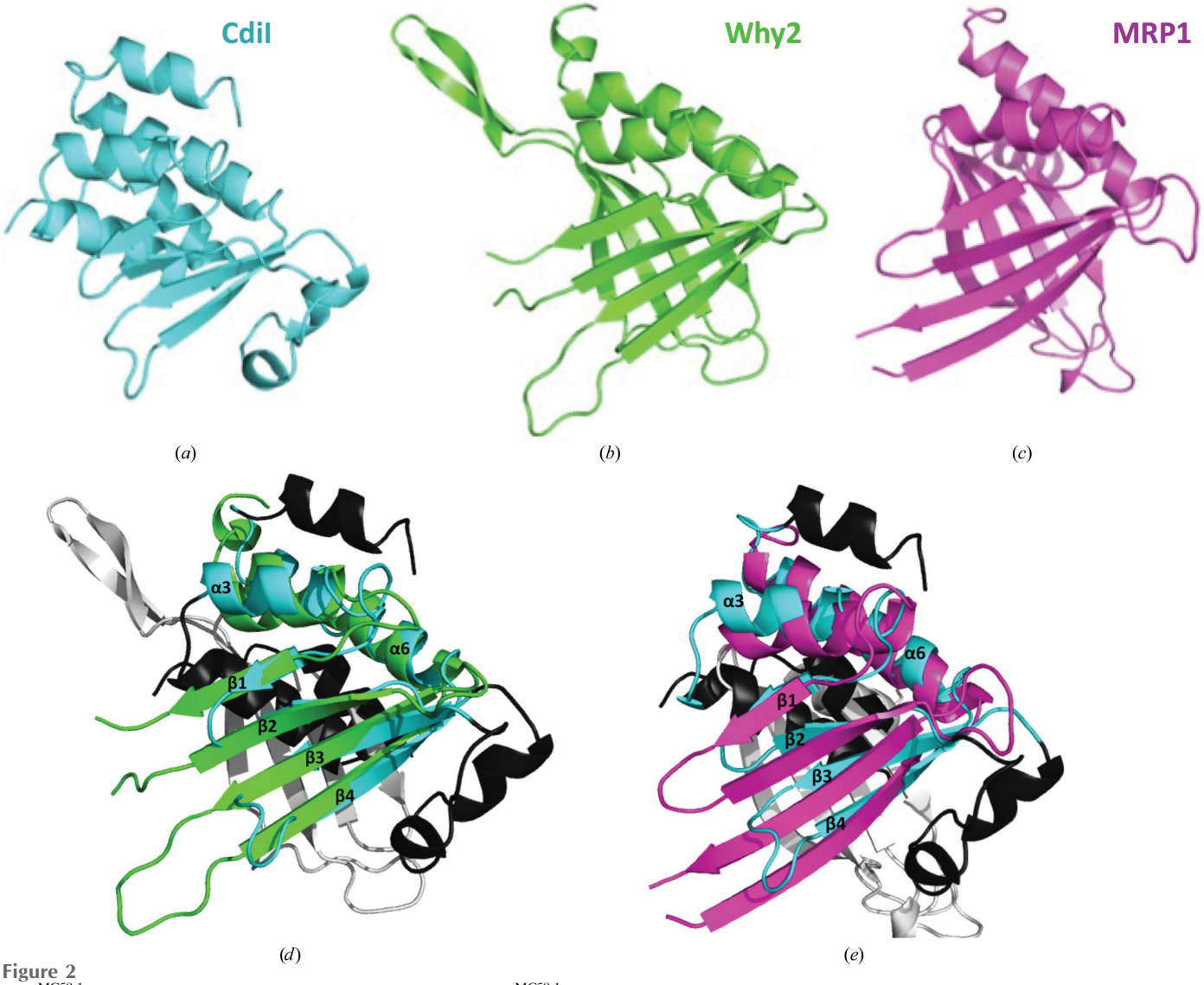

Figure 2
CdiI$_{o2}^{MC58\text{-}1}$ structural homologs in ribbon representation. (*a*) CdiI$_{o2}^{MC58\text{-}1}$ (PDB entry 4q7o), (*b*) Why2 (PDB entry 4kop) and (*c*) MRP1 (PDB entry 2gia). (*d*) Superimposition of CdiI$_{o2}^{MC58\text{-}1}$ and Why2. Secondary-structure elements of CdiI$_{o2}^{MC58\text{-}1}$ and Why2 that superimpose with good agreement are colored cyan and green, respectively. Structural elements that do not superimpose are colored black and white for CdiI$_{o2}^{MC58\text{-}1}$ and Why2, respectively. (*e*) Superimposition of CdiI$_{o2}^{MC58\text{-}1}$ and MRP1. Secondary-structure elements of CdiI$_{o2}^{MC58\text{-}1}$ and MRP1 that superimpose with good agreement are colored cyan and pink, respectively. Structural elements that do not superimpose are colored black and white for CdiI$_{o2}^{MC58\text{-}1}$ and MRP1, respectively.

elements used by these proteins to bind DNA or RNA. These observations suggest that CdiI$_{o2}^{MC58-1}$ is unlikely to bind nucleic acids.

3.3. Predicted function of the CdiA-CT$_{o2}^{MC58-1}$ toxin

No experimental or structural information is available for CdiA-CT$_{o2}^{MC58-1}$, which is the predicted toxin encoded by the adjacent NMB0502 gene. Aravind and coworkers have predicted that the C-terminal domain of CdiA-CT$_{o2}^{MC58-1}$ is related to the EndoU nucleases (Zhang *et al.*, 2012), which comprise a superfamily of Mn^{2+}-dependent RNA-processing enzymes found mostly in eukaryotes, although family members are also found in the cyanobacterium *Nostoc punctiforme* (Renzi *et al.*, 2006) and at the C-terminus of a MafB RNase toxin from *N. meningitidis* (Jamet *et al.*, 2015). CdiA-CT$_{o2}^{MC58-1}$ has diverged substantially from the eukaryotic enzymes and shares only 16% sequence identity with the C-terminal nuclease domain (residues Ile142–Tyr292) of XendoU, a poly(U)-specific endoribonuclease from *Xenopus laevis* (Fig. 3*a*; Laneve *et al.*, 2003). The crystal structure of XendoU has been solved (Renzi *et al.*, 2006), and therefore we used it as a guide to generate a model of CdiA-CT$_{o2}^{MC58-1}$ (Fig. 3*c*). The resulting model shows that the XendoU active-

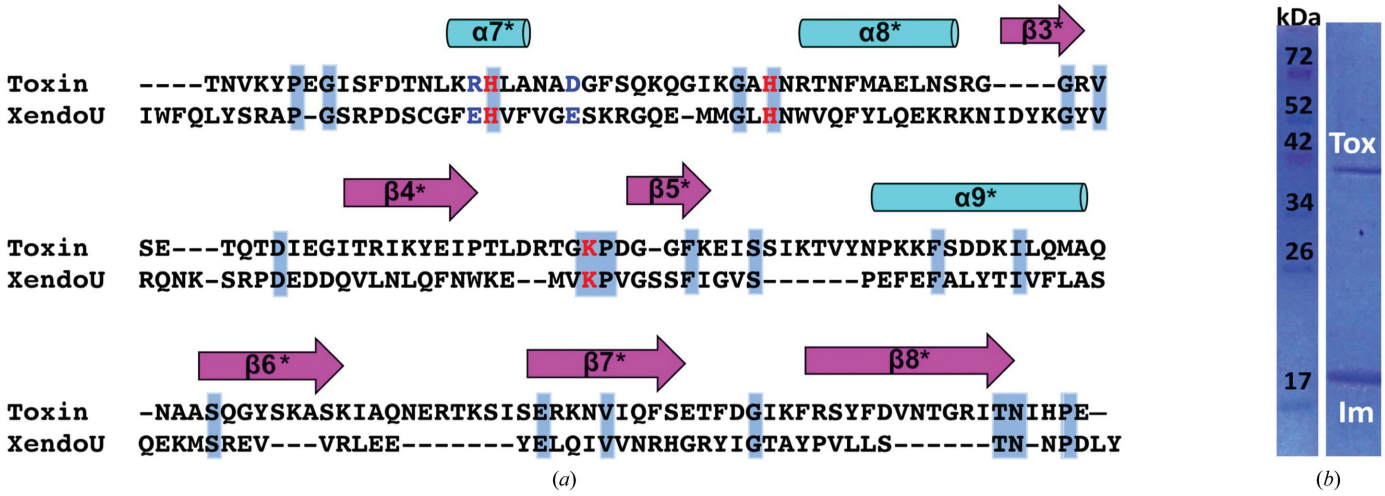

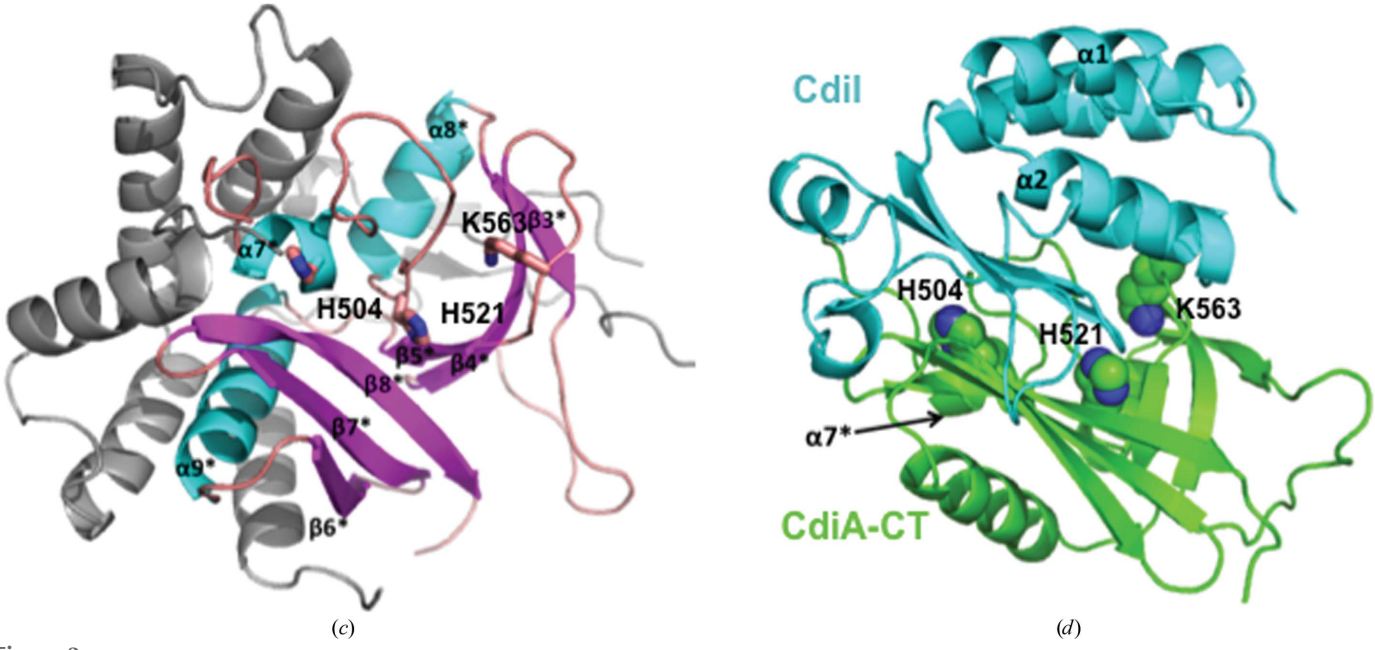

Figure 3
Modeled structures of CdiA-CT$_{o2}^{MC58-1}$ and its complex with CdiI$_{o2}^{MC58-1}$. (*a*) Sequence alignment by *ClustalW* of the C-terminal region of CdiA-CT$_{o2}^{MC58-1}$ with the C-terminal domain of XendoU (PDB entry 2c1w). Residues on a gray/blue background are conserved, catalytic residues are colored red and RNA-binding residues are colored blue. (*b*) SDS–PAGE of the Ni^{2+}-affinity purified complex of untagged CdiA-CT$_{o2}^{MC58-1}$ (Tox) with His_6-tagged CdiI$_{o2}^{MC58-1}$ (Im). (*c*) Modeled structure of the C-terminal domain of CdiA-CT$_{o2}^{MC58-1}$ with α-helices colored cyan and β-strands colored salmon. Elements in light gray are those of the N-terminal domain of the XendoU structure that have no sequence homology to CdiA-CT$_{o2}^{MC58-1}$. The predicted active-site residues of CdiA-CT$_{o2}^{MC58-1}$ are shown in stick representation with C, O and N atoms colored pink, red and blue, respectively. (*d*) The docked complex structure in ribbon representation of the toxin (colored green, secondary-structure elements indicated with asterisks) with the immunity protein (colored cyan). The predicted CdiA-CT$_{o2}^{MC58-1}$ active-site residues, shown in sphere representation with C and N atoms colored green and blue, respectively, are occluded from solvent by the docked immunity protein CdiI$_{o2}^{MC58-1}$.

site residues His162, His178 and Lys224 correspond to His504, His521 and Lys563 in CdiA-CT$_{o2}^{MC58-1}$ (Renzi *et al.*, 2006; Gioia *et al.*, 2005). Together, these observations suggest that CdiA-CT$_{o2}^{MC58-1}$ may possess a similar Mn^{2+}-dependent RNA-processing/degrading activity to other members of the EndoU family.

3.4. Modeling of the CdiA-CT$_{o2}^{MC58-1}$–CdiI$_{o2}^{MC58-1}$ complex

To gain insight into the toxin–immunity protein binding interactions, we first tested whether CdiA-CT$_{o2}^{MC58-1}$ forms a complex with CdiI$_{o2}^{MC58-1}$. We co-expressed the toxin with His_6-tagged CdiI$_{o2}^{MC58-1}$ (as described in §2.6) and then purified the immunity protein by Ni^{2+}-affinity chromatography. The untagged toxin co-eluted with His_6-tagged CdiI$_{o2}^{MC58-1}$ (Fig. 3*b*), indicating that CdiA-CT$_{o2}^{MC58-1}$ and CdiI$_{o2}^{MC58-1}$ do indeed form a complex. We then conducted docking simulations of the monomeric CdiI$_{o2}^{MC58-1}$ immunity protein structure onto the CdiA-CT$_{o2}^{MC58-1}$ model. The lowest interaction energy obtained from these simulations was −776.7 kcal mol^{-1}, which is considerably lower than the energy calculated for non-interacting proteins as described in §2. The *Hex*-generated model predicts that CdiI$_{o2}^{MC58-1}$ binds directly over the active site of CdiA-CT$_{o2}^{MC58-1}$ (Fig. 3*d*), likely neutralizing the toxin by preventing access to RNA substrates.

4. Conclusions

We have elucidated the structure of CdiI$_{o2}^{MC58-1}$, a predicted immunity protein encoded within the CDI-1 locus of *N. meningitidis* MC58. CdiI$_{o2}^{MC58-1}$ has moderate structural homology to Whirly-like proteins found in plastids, but appears to lack the characteristic Whirly RNA-binding site. In addition, we modeled the structure of the associated CdiA-CT$_{o2}^{MC58-1}$ toxin domain, which is proposed to have a similar active-site motif and RNA-processing activity as eukaryotic EndoU nucleases. Molecular-docking simulations predict that CdiI$_{o2}^{MC58-1}$ occludes the active site of CdiA-CT$_{o2}^{MC58-1}$ in the toxin–immunity protein complex. Experiments to test the biochemical activity of CdiA-CT$_{o2}^{MC58-1}$ and its proposed active-site residues are under way.

Acknowledgements

This research was supported by National Institutes of Health grants GM102318 (to CWG, CSH and subcontract to Argonne) and GM094585 (to AJ). The use of SBC beamlines was supported by the US Department of Energy, Office of Biological and Environmental Research under contract DE-AC02-06CH11357.

References

Afonine, P. V., Grosse-Kunstleve, R. W., Echols, N., Headd, J. J., Moriarty, N. W., Mustyakimov, M., Terwilliger, T. C., Urzhumtsev, A., Zwart, P. H. & Adams, P. D. (2012). *Acta Cryst.* D**68**, 352–367.

Aoki, S. K., Diner, E. J., t'Kint de Roodenbeke, C., Burgess, B. R., Poole, S. J., Braaten, B. A., Jones, A. M., Webb, J. S., Hayes, C. S., Cotter, P. A. & Low, D. A. (2010). *Nature (London)*, **468**, 439–442.

Aoki, S. K., Pamma, R., Hernday, A. D., Bickham, J. E., Braaten, B. A. & Low, D. A. (2005). *Science*, **309**, 1245–1248.

Aoki, S. K., Poole, S. J., Hayes, C. S. & Low, D. A. (2011). *Virulence*, **2**, 356–359.

Aphasizhev, R., Aphasizheva, I., Nelson, R. E. & Simpson, L. (2003). *RNA*, **9**, 62–76.

Arenas, J., Schipper, K., van Ulsen, P., van der Ende, A. & Tommassen, J. (2013). *BMC Genomics*, **14**, 622.

Bentley, S. D. *et al.* (2007). *PLoS Genet.* **3**, e23.

Birmanns, S., Rusu, M. & Wriggers, W. (2011). *J. Struct. Biol.* **173**, 428–435.

Cappadocia, L., Maréchal, A., Parent, J.-S., Lepage, E., Sygusch, J. & Brisson, N. (2010). *Plant Cell*, **22**, 1849–1867.

Cappadocia, L., Parent, J.-S., Sygusch, J. & Brisson, N. (2013). *Acta Cryst.* F**69**, 1207–1211.

Cohen, S. X., Morris, R. J., Fernandez, F. J., Ben Jelloul, M., Kakaris, M., Parthasarathy, V., Lamzin, V. S., Kleywegt, G. J. & Perrakis, A. (2004). *Acta Cryst.* D**60**, 2222–2229.

Dauter, Z., Dauter, M. & Rajashankar, K. R. (2000). *Acta Cryst.* D**56**, 232–237.

Desveaux, D., Maréchal, A. & Brisson, N. (2005). *Trends Plant Sci.* **10**, 95–102.

Diner, E. J., Beck, C. M., Webb, J. S., Low, D. A. & Hayes, C. S. (2012). *Genes Dev.* **26**, 515–525.

Emsley, P. & Cowtan, K. (2004). *Acta Cryst.* D**60**, 2126–2132.

Eschenfeldt, W. H., Makowska-Grzyska, M., Stols, L., Donnelly, M. I., Jedrzejczak, R. & Joachimiak, A. (2013). *J. Struct. Funct. Genomics*, **14**, 135–144.

Eschenfeldt, W. H., Maltseva, N., Stols, L., Donnelly, M. I., Gu, M., Nocek, B., Tan, K., Kim, Y. & Joachimiak, A. (2010). *J. Struct. Funct. Genomics*, **11**, 31–39.

Gioia, U., Laneve, P., Dlakic, M., Arceci, M., Bozzoni, I. & Caffarelli, E. (2005). *J. Biol. Chem.* **280**, 18996–19002.

Gupta, U. K., Mahanta, S. & Paul, S. (2013). *Med. Hypotheses*, **81**, 853–861.

Holm, L., Kääriäinen, S., Rosenström, P. & Schenkel, A. (2008). *Bioinformatics*, **24**, 2780–2781.

Jamet, A., Jousset, A. B., Euphrasie, D., Mukorako, P., Boucharlat, A., Ducousso, A., Charbit, A. & Nassif, X. (2015). *PLoS Pathog.* **11**, e1004592.

Kajava, A. V., Cheng, N., Cleaver, R., Kessel, M., Simon, M. N., Willery, E., Jacob-Dubuisson, F., Locht, C. & Steven, A. C. (2001). *Mol. Microbiol.* **42**, 279–292.

Koskiniemi, S., Garza-Sánchez, F., Sandegren, L., Webb, J. S., Braaten, B. A., Poole, S. J., Andersson, D. I., Hayes, C. S. & Low, D. A. (2014). *PLoS Genet.* **10**, e1004255.

Krissinel, E. & Henrick, K. (2007). *J. Mol. Biol.* **372**, 774–797.

Laneve, P., Altieri, F., Fiori, M. E., Scaloni, A., Bozzoni, I. & Caffarelli, E. (2003). *J. Biol. Chem.* **278**, 13026–13032.

Macindoe, G., Mavridis, L., Venkatraman, V., Devignes, M. D. & Ritchie, D. W. (2010). *Nucleic Acids Res.* **38**, W445–W449.

Minor, W., Cymborowski, M., Otwinowski, Z. & Chruszcz, M. (2006). *Acta Cryst.* D**62**, 859–866.

Nikolakakis, K., Amber, S., Wilbur, J. S., Diner, E. J., Aoki, S. K., Poole, S. J., Tuanyok, A., Keim, P. S., Peacock, S., Hayes, C. S. & Low, D. A. (2012). *Mol. Microbiol.* **84**, 516–529.

Nikulin, J., Panzner, U., Frosch, M. & Schubert-Unkmeir, A. (2006). *Int. J. Med. Microbiol.* **296**, 553–558.

Norel, R., Lin, S. L., Wolfson, H. J. & Nussinov, R. (1995). *J. Mol. Biol.* **252**, 263–273.

Poole, S. J., Diner, E. J., Aoki, S. K., Braaten, B. A., t'Kint de Roodenbeke, C., Low, D. A. & Hayes, C. S. (2011). *PLoS Genet.* **7**, e1002217.

Renzi, F., Caffarelli, E., Laneve, P., Bozzoni, I., Brunori, M. & Vallone, B. (2006). *Proc. Natl Acad. Sci. USA*, **103**, 12365–12370.

Rosenbaum, G. *et al.* (2006). *J. Synchrotron Rad.* **13**, 30–45.
Ruhe, Z. C., Low, D. A. & Hayes, C. S. (2013). *Trends Microbiol.* **21**, 230–237.
Ruhe, Z. C., Nguyen, J. Y., Beck, C. M., Low, D. A. & Hayes, C. S. (2014). *Mol. Microbiol.* **94**, 466–481.
Schumacher, M. A., Karamooz, E., Zíková, A., Trantírek, L. & Lukeš, J. (2006). *Cell*, **126**, 701–711.
Sheldrick, G. M. (2008). *Acta Cryst.* A**64**, 112–122.
Thigpen, M. C. *et al.* (2011). *N. Engl. J. Med.* **364**, 2016–2025.
Winn, M. D. *et al.* (2011). *Acta Cryst.* D**67**, 235–242.
Zhang, D., de Souza, R. F., Anantharaman, V., Iyer, L. M. & Aravind, L. (2012). *Biol. Direct*, **7**, 18.